EGU General Assembly 2023, Vienna, Austria & Online | 23–28 April 2023
Session: GMPV9.1/NH2.10
EGU23-2186

Volcanism of Mount Fuji activated by the 2011 Japanese large earthquakes

*K. Z. Nanjo (Univ. Shizuoka, Japan), Y. Yukutake (Univ. Tokyo, Japan), T. Kumazawa (Inst. Stat. Math., Japan)

https://doi.org/10.5194/egusphere-egu23-2186

The relation between earthquakes and volcanic eruptions, each of which is manifested by large-scale tectonic plate and mantle motions, has been widely discussed. Mount Fuji in Japan last erupted in 1707, paired with a magnitude (*M*)-9-class earthquake that took place 49 days prior. Motivated by this pairing, previous studies examined the effect of both the 2011 *M*9 Tohoku megaquake and a triggered *M*6-class earthquake 4 days later at the foot of the volcano on Mount Fuji, although no volcanic eruption was reported. More than 300 years already have passed since the last 1707 eruption, and although consequences to humans and society caused by the next eruption are already being considered, the implication for future volcanism remains uncertain. Here we show how volcanic low-frequency earthquakes (LFEs) in the deep part of the volcano revealed hitherto-unrecognized activation immediately after the foot earthquake. Our analyses using statistical methods based on the matched-filtering and the epidemic-type aftershock sequence (ETAS) show that despite an increase in the rate of occurrence of LFEs, these did not return to pre-earthquake levels, indicating a change in the magma system. Our results demonstrate that the volcanism of Mount Fuji was reactivated by the foot earthquake, implying that this volcano is sufficiently sensitive to external events that are enough to trigger eruptions.

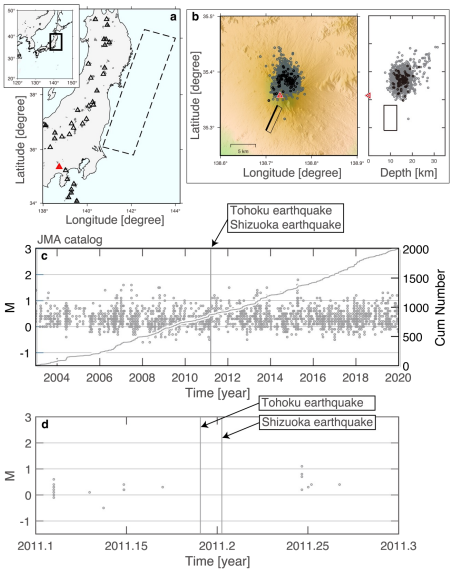

Fig. 1| Mount Fuji and Japanese earthquakes. a, Map showing Mount Fuji (red triangle) and the source area of the Tohoku earthquake (rectangular area surrounded by broken lines). Active volcanoes are indicated by black triangles. Grey dots indicate LFEs in the Japan Meteorological Agency (JMA) catalog. **b**, Left panel shows LFEs (grey circles) around Mount Fuji (summit is indicated by a triangle). Black circles indicate 87 template LFEs. The source area of the Shizuoka earthquake is indicated by a rectangular area. Right panel shows a cross-sectional view of the LFEs and the source area. **c**, M-time diagram of LFEs (y-axis on the left side). Overlapped is the cumulative number of LFEs as a function of time since 2003 (y-axis on the right side). Vertical line indicates the moments of the Tohoku and Shizuoka earthquakes, which overlap. **d**, Same as **c** for a zoom-in plot at times before and after both earthquakes from 2011.1, as a decimal year (Feb. 6, 2011, 12:00:00) to 2011.3, as a decimal year (Apr. 20, 2011, 12:00:00).

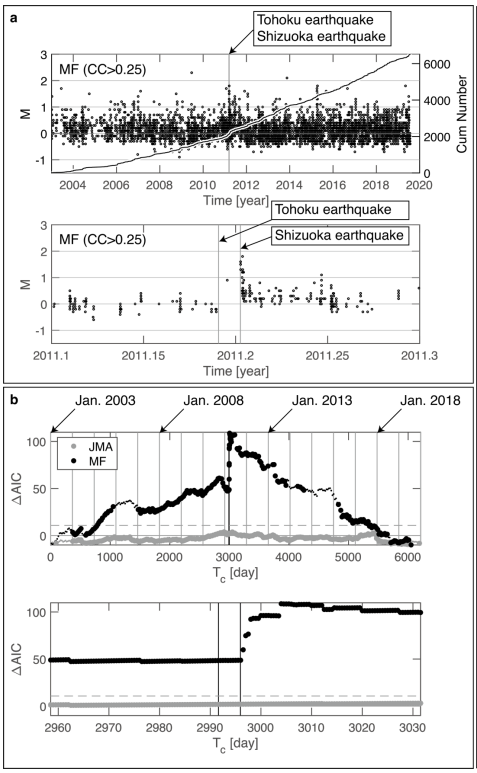

Fig. 2| MF method of LFEs. a, Same as Fig. 1**c**,**d** for LFEs in the Matched Filter (MF) catalog (*CC*>0.25). The MF system used for detecting LFEs beneath the Hakone volcano, Japan (Yukutake et al., 2019) was modified so that it was applicable to Mount Fuji. **b**, Top panel: $\Delta AIC = AIC_{single} - AIC_{2stage}$ as a function of T_c since 2003, where LFEs (*M*≥0.3) in the MF catalog (*CC*>0.25) (black) and LFEs (*M*≥0.5) in the JMA catalog (grey) were used. The minimum magnitudes (M_{th}=0.3 and 0.5) for the MF and JMA catalogs, respectively, were used, taking homogeneity of seismicity recordings of both catalogs into consideration. Small points show that the model-fitting analysis did not converge when assuming the corresponding T_c. As a reference, thin vertical lines indicate Jan. 1 for 2004-2019. The timings of the Tohoku and Shizuoka earthquakes overlap, showing a single thick vertical line. Horizontal dashed lines representing 2*q* for the MF and JMA catalogs overlap, where *q* is the degree of freedom imposed when searching T_c based on the data over the entire period (Kumazawa et al., 2019). Bottom panel: same as the top panel for zoom-in from Feb. 6, 2011, 12:00:00 to Apr. 20, 2011, 12:00:00.

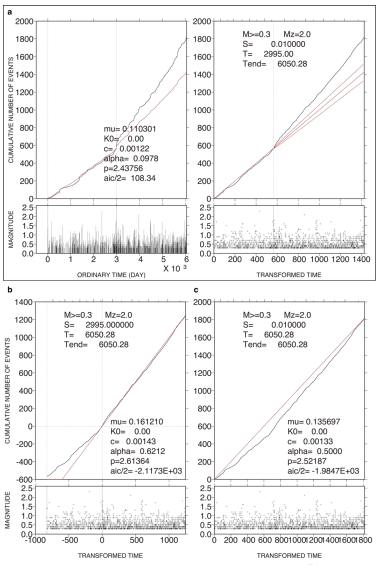

Fig. 3| Change point analysis of LFEs. a, Cumulative function and *M*≥0.3 are plotted against ordinary time (left panel) and transformed time (right panel), showing the ETAS fitting in the target interval from 2003 until immediately before the Shizuoka earthquake and then extrapolated until July 2019. The parabola represents the 95% confidence intervals of the extrapolation. Note that K_0=4.51×10^{-5} for *M*=2, although "K_0=0.00" is shown in the graph. The smaller panel below each larger panel indicates an *M*-time diagram. **b**, As in **a** except that the target is the later time interval after the Shizuoka earthquake. Because K_0=6.16×10^{-5} obtained is too small, it is shown as "K_0=0.00" in the graph. **c**, As in **a** except that the target is the entire time interval.

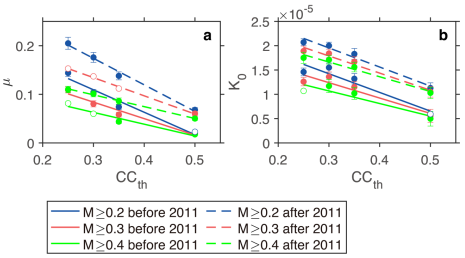

Fig. 4| Background and aftershock seismicity. a,**b**, μ and K_0 as a function of CC_{th}, calculated for two time-windows before Jan. 1, 2011 (solid line) and after Dec. 31 2011 (broken line). We considered the minimum magnitudes M_{th}=0.2 (blue), 0.3 (red), and 0.4 (green). Other ETAS parameters (*c*, *p*, and α) are constants irrespective of different values for time windows, M_{th}, and CC_{th}: (*c*, *p*, α)=(0.0015, 2.80, 0.5). Open circles indicate that the model-fitting analysis did not converge well, resulting in large errors.

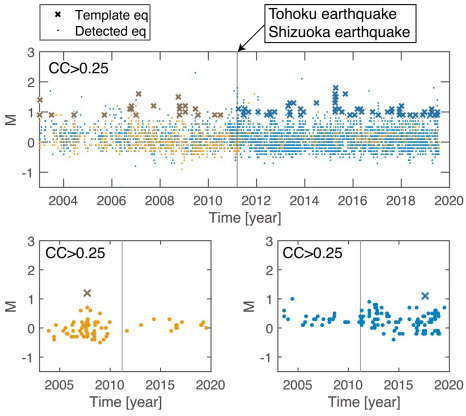

Fig. 5| Temporal changes of LFE pattern. Top panel: same as Fig. 2**a** except for the separation between LFEs (orange dots) detected by a correlation with waveforms of template LFEs (orange cross) listed in the JMA catalog before the Tohoku earthquake and LFEs (blue dots) by a correlation with waveforms of template LFEs (blue cross) after the Shizuoka earthquake. Bottom left panel: same as the top panel for highlighting LFEs detected by using an exemplified template LFE before the Tohoku and Shizuoka earthquakes (vertical line). Bottom right panel: same as the bottom left panel, but after these earthquakes.

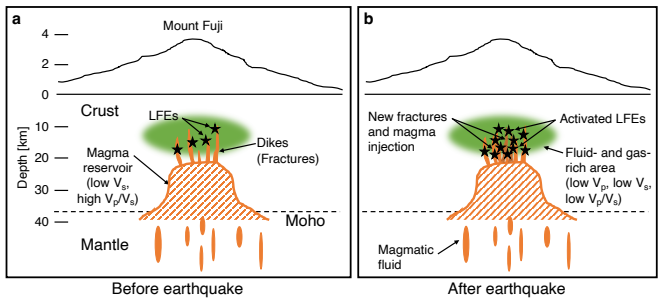

Fig. 6| Schematic cross sections. Relationship between LFEs and the magma system beneath Mount Fuji, before and after the Shizuoka earthquake, is shown in **a** and **b**, respectively. **a** is based on previous studies (Ukawa, 2005; Nakamichi et al., 2007). New fractures and magma injection due to the earthquake were suggested (Fujita et al., 2013), shown in **b**. We proposed activated LFEs in **b**.

Acknowledgments
This study was partially supported by the Ministry of Education, Culture, Sports, Science and Technology (MEXT) of Japan, under The Second Earthquake and Volcano Hazards Observation and Research Program (Earthquake and Volcano Hazard Reduction Research) (K.Z.N., Y.Y.) and under STAR-E (Seismology TowArd Research innovation with data of Earthquake) Program Grant Number JPJ010217 (K.Z.N., T.K.), JSPS KAKENHI Grant Number JP 20K05050 (K.Z.N.), 21K04613 (K.Z.N.), 22K03752 (Y.Y.), 20K11704 (T.K.), the Chubu Electric Power's research based on selected proposals (K.Z.N.), the Consortium of Universities & Local Communities in Shizuoka (K.Z.N., Y.Y.), and the WNI W-Bunka Foundation (K.Z.N.). The authors thank Y. Noda for help with implementing the MF method.

Supplementary Fig. S3. Change point analysis. **a**, Left panels: ΔAIC as a function of T_c for different minimum magnitudes (M_{th}=0.2, 0.3, and 0.4) of LFEs obtained for the MF method (CC>0.25, 0.3, 0.35, and 0.5). Right panels: Same as the left panels for zoom-in at times before and after the Tohoku and Shizuoka earthquakes. In the left panel of CC>0.35, ΔAIC-values above the horizontal dashed lines for T_c≤290 were

interpreted to be less reliable because the model-fitting analysis converged to a local optimal solution. **b**, Same as the left panels of **a** for the JMA catalog (M_{th}=0.3, 0.4, and 0.5).

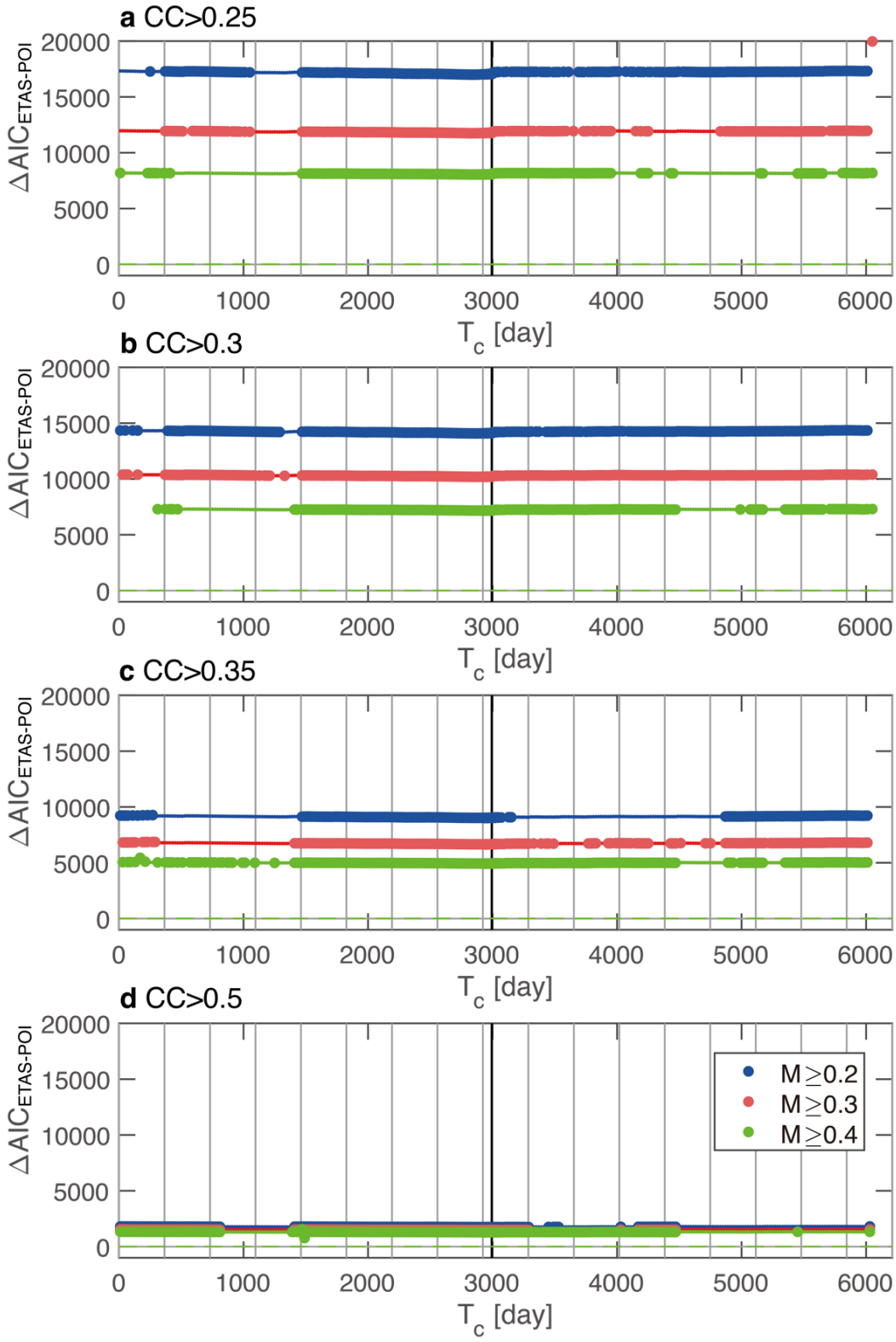

Supplementary Fig. S4. Comparison between the two-stage ETAS and Poisson models.

The latter model is the same as the former, except for K_0=0. This model assumes different parameter values for μ in subperiods before and after T_c. Subtraction of AIC_{2stage} (AIC for the two-stage ETAS model) from AIC for the two-stage Poisson model gives $\Delta AIC_{ETAS\text{-}POI}$. **a**, $\Delta AIC_{ETAS\text{-}POI}$ (CC>0.25) as a function of T_c for different values of the minimum magnitudes: M_{th}=0.2 (blue), 0.3 (red) and 0.4 (green). Small points show that the model-fitting analysis did not converge for either or both of the models when assuming the corresponding T_c. **b**,**c**,**d**, Same as **a** for CC>0.3, 0.35, and 0.5, respectively. Also see the captions of Fig. 2 and Supplementary Fig. S3.

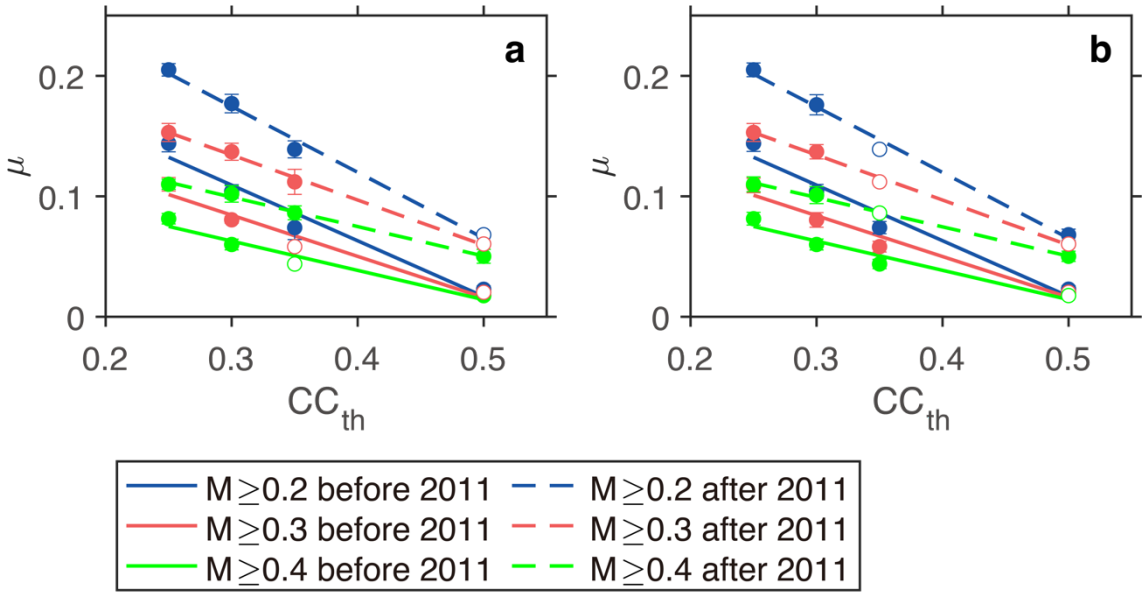

Supplementary Fig. S5. Sensitivity test of the μ-CC_{th} pattern. **a**, Same as Fig. 4**a** except that sets of parameters were prefixed as follows: (α, K_0, c)=(0.5, 10^{-5}, 0.0015). The slope (g) and intersection (h) of the least-square regression line and the square of the sample correlation coefficient (R^2) are $\mu=gCC_{th}+h$ with (g, h, R^2)=(-0.46, 0.25, 0.96) for M≥0.2 (blue solid line), (-0.34, 0.19, 0.96) for M≥0.3 (red solid line), and (-0.24, 0.14, 0.95) for M≥0.4 (green solid line) before 2011, and (-0.55, 0.34, 0.99) for M≥0.2 (blue dashed line), (-0.37, 0.25, 1.00) for M≥0.3 (red dashed line), and (-0.24, 0.17, 1.00) for M≥0.4 (green dashed line) after 2011. **b**, Same as **a** except that the sets of parameters were prefixed as follows: (K_0, c, p)=(10^{-5}, 0.0015, 2.8). $\mu=gCC_{th}+h$ with (g, h, R^2)=(-0.46, 0.25, 0.96) for M≥0.2 (blue solid line), (-0.34, 0.19, 0.96) for M≥0.3 (red

solid line), and (-0.24, 0.14, 0.95) for $M \geq 0.4$ (green solid line) before 2011, and (-0.55, 0.34, 0.99) for $M \geq 0.2$ (blue dashed line), (-0.37, 0.25, 1.00) for $M \geq 0.3$ (red dashed line), and (-0.24, 0.17, 1.00) for $M \geq 0.4$ (green dashed line) after 2011. See the caption of Fig. 3.

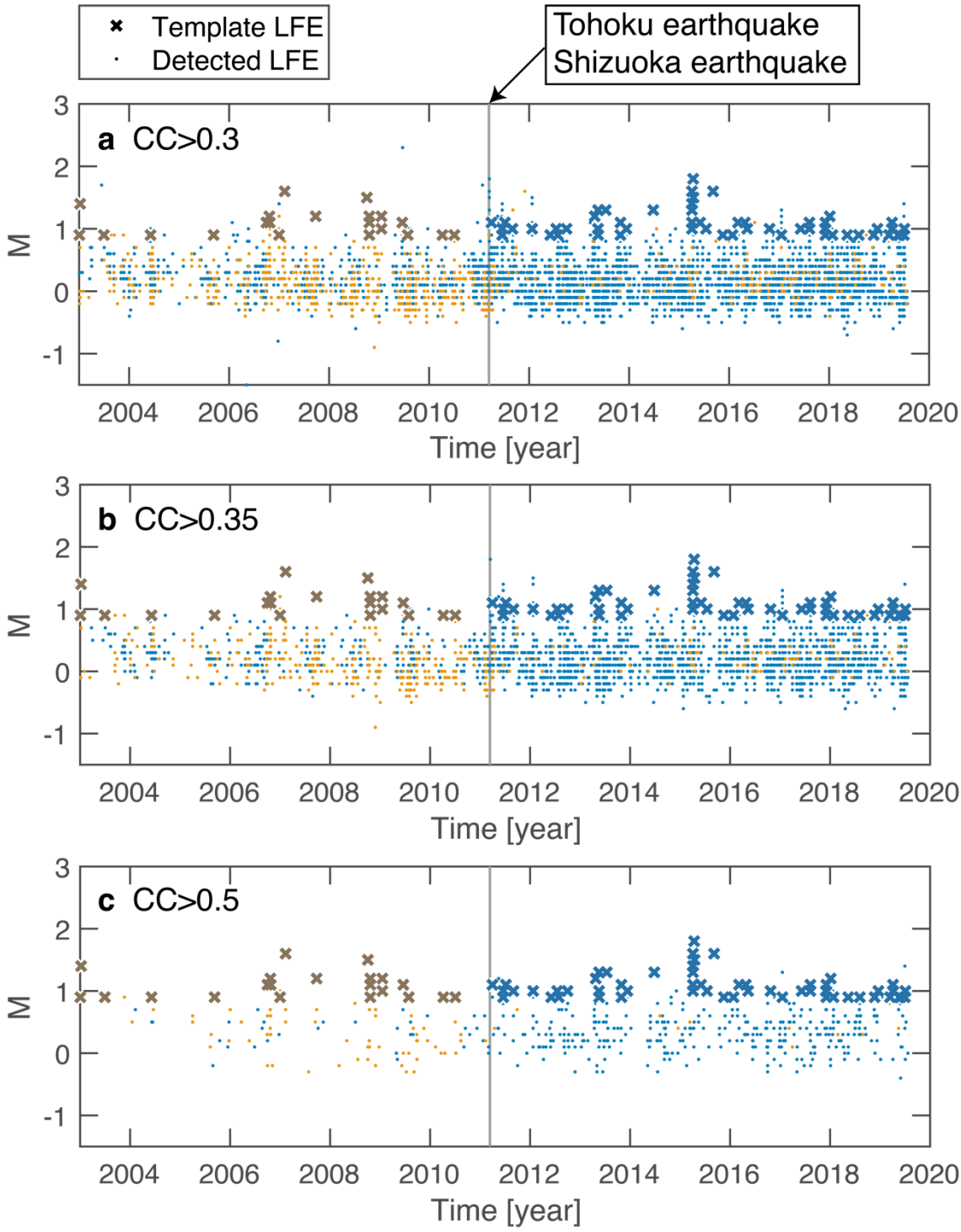

Supplementary Fig. S6. Same as the top panel of Fig. 5 for *CC*>0.3 in **a**, 0.35 in **b**, and 0.5 in **c**. Also see the caption of Fig. 5.

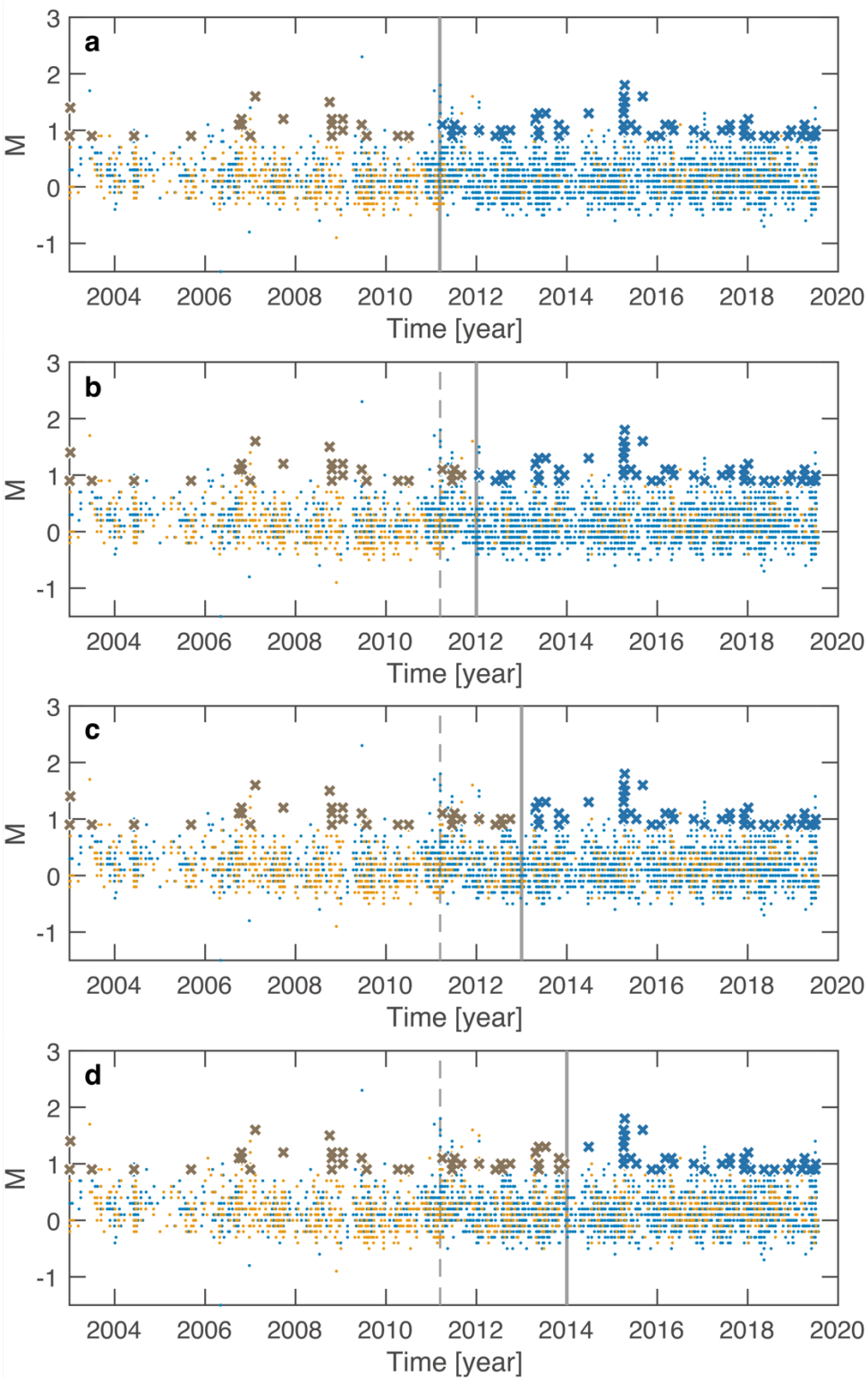

Supplementary Fig. S7. Same as Fig. 5 except for the time-windows, which were

defined differently. **a**, Same graph as the top panel of Fig. 5. The same test as **a** was conducted for a time-limit (vertical solid line) before and after 2012 in **b**, 2013 in **c**, and 2014 in **d**. Vertical dotted line indicates the moments of Tohoku and Shizuoka earthquakes, which overlap with each other. In **a**, the majority of LFEs in the time-window after the time-limit appears to be colored in blue. Since the time-limit was set to 2014 in **d**, the majority of LFEs in the same time-window appears to be colored in both blue and orange. This indicates that templates (crosses) until 2014 from the moments of the Tohoku and Shizuoka earthquakes contributed to the detection of LFEs (dots) after 2014. These results support our statement that LFEs before/after the moments of the Tohoku and Shizuoka earthquakes were mostly detected by templates in the same time periods.